Binding interaction of SARS coronavirus 3CL^{pro} protease with vacuolar-H$^+$ ATPase G1 subunit

Cheng-Wen Lin[a,b,*], Fuu-Jen Tsai[c], Lei Wan[c], Chien-Chen Lai[c], Kuan-Hsun Lin[a], Tsung-Han Hsieh[a], Shi-Yi Shiu[a], Jeng-Yi Li[a]

[a] *Department of Medical Laboratory Science and Biotechnology, China Medical University, No. 91, Hsueh-Shih Road, Taichung 404, Taiwan*
[b] *Clinical Virology Laboratory, Department of Laboratory Medicine, China Medical University Hospital, Taichung 404, Taiwan*
[c] *Department of Medical Genetics and Medical Research, China Medical University Hospital, Taichung 404, Taiwan*

Received 17 August 2005; revised 18 September 2005; accepted 19 September 2005

Available online 6 October 2005

Edited by Michael R. Bubb

Abstract The pathogenesis of severe acute respiratory syndrome coronavirus (SARS-CoV) is an important issue for treatment and prevention of SARS. Recently, SARS-CoV 3CL^{pro} protease has been implied to be possible relevance to SARS-CoV pathogenesis. In this study, we intended to identify potential 3CL^{pro}-interacting cellular protein(s) using the phage-displayed human lung cDNA library. The vacuolar-H$^+$ ATPase (V-ATPase) G1 subunit that contained a 3CL^{pro} cleavage site-like motif was identified as a 3CL^{pro}-interacting protein, as confirmed using the co-immunoprecipitation assay and the relative affinity assay. In addition, our result also demonstrated the cleavage of the V-ATPase G1 fusion protein and the immunoprecipitation of cellular V-ATPase G1 by the 3CL^{pro}. Moreover, loading cells with SNARF-1 pH-sensitive dye showed that the intracellular pH in 3CL^{pro}-expressing cells was significantly lower as compared to mock cells.

Keywords: SARS-coronavirus; 3CL^{pro}; Vacuolar-H$^+$ ATPase G1; Phage display; Human lung cDNA libraries

1. Introduction

Severe acute respiratory syndrome-associated coronavirus (SARS-CoV) causes bronchial epithelial denudation, loss of cilia, and multinucleated in lung tissues [1,2], and induces lymphopenia, leucopenia, and thrombocytopenia in the SARS patients [3,4]. The relevance to SARS-CoV pathogenesis becomes an attractive issue for developing anti-SARS therapy. SARS-CoV contains a single positive-stranded RNA genome that is approximately 30 kb in length and has a 5′ cap structure and 3′ polyA tract [5–7]. The SARS-CoV genome encodes for replicase, spike, envelope, membrane, and nucleocapsid. The replicase gene encodes two large overlapping polypeptides (replicase 1a and 1ab, ~450 and ~750 kD, respectively), including 3C-like protease (3CL^{pro}), RNA-dependent RNA polymerase, and RNA helicase for viral replication and transcription [8]. The SARS-CoV 3CL^{pro} mediates the proteolytic processing of replicase polypeptides 1a and 1ab into functional proteins, thereby playing an important role in viral replication. In the case of picornaviruses, poliovirus, enterovirus 71, and rhinovirus, 3C protease have been demonstrated to cleave specific cellular proteins [9,10], inhibit the cellular translation [11,12], and induce cell apoptosis [13–15]. Recently, SARS-CoV 3CL^{pro} cleavage sites have been predicted in cellular proteins such as the cystic fibrosis transmembrane conductance regulator, and transcription factors CREB-RP and OCT-1 using computational methods [16], signifying SARS-CoV 3CL^{pro} protease can be involved in virus-induced pathology. In this study, we intended to identify potential 3CL^{pro}-interacting cellular protein(s) using the phage-displayed human lung cDNA library.

2. Materials and methods

2.1. Biopanning of phage display lung cDNA libraries with SARS-CoV 3CL^{pro}

The 3CL^{pro}-expressing *E. coli* strain described in our previous report [17] was used for generation of recombinant 3CL^{pro} His-tag fusion protein. For biopanning, the T7Select human lung cDNA library fused at the C terminus of phage capsid protein 10B was purchased from Novagen (Madison, WI). Following the biopanning procedure in our previous report [18], five rounds of biopanning for screening 3CL^{pro}-affinity phage clones were carried out using 3CL^{pro}-coated microplates (5 μg per well). The 3CL^{pro}-affinity phage clones were eluted with the soluble 3CL^{pro}. For direct ELISA binding assay, the individual eluted phage clones that were determined using a plaque assay were coated onto microplates (10^{10} p.f.u./well) for 1 h at room temperature. After blocking phage-coated plates, 100 μl of 20 μg/ml 3CL^{pro} was added to each well for additional 1-h incubation. Bound 3CL^{pro} was detected using the ELISA with the anti-His tag monoclonal antibody and anti-mouse IgG antibodies conjugated to peroxidase (Pharmacia). ELISA product was developed with a chromogen solution containing ABTS (2,2′-azino-di-(3-ethylbenzthiazoline-6-sulfonate)) and hydrogen peroxide and then measured at $A_{405\ nm}$. The lung cDNA genes displayed on 3CL^{pro}-affinity phages were directly amplified using PCR with the T7 Select UP primer 5′-GGAGCTGTCGTATTCCAGTCA-3′ and the T7 Select DOWN primer 5′-CCCCTCAAGACCCGTTTA-3′. The nucleotide sequences of each PCR product were determined using the sequencing with the ABI PRISM 377 DNA Sequencer (Perkin–Elmer, USA). The deduced amino acid sequences of 3CL^{pro}-interacting lung cDNA clones were aligned using the BLAST search (http://www.ncbi.nlm.nih.gov/BLAST/).

2.2. Co-immunoprecipitation of SARS-CoV 3CL^{pro} protease by vacuolar-H$^+$ ATPase G1 subunit

For the cell-free co-immunoprecipitation assay, the vacuolar-H$^+$ ATPase gene was cloned into the vector pET32a, and expressed as the fusion protein with thioredoxin (Trx) at the N-terminus and

*Corresponding author. Fax: +886 4 22057414.
E-mail address: cwlin@mail.cmu.edu.tw (C.-W. Lin).

0014-5793/$30.00
doi:10.1016/j.febslet.2005.09.075

His-tag at the C-terminus. The cDNA of the C-terminal vacuolar-H^+ ATPase subunit G1 displayed on the $3CL^{pro}$-affinity phage clone 7 was amplified by PCR with primers: 5′-ATCCGAATTCGCCAAG-GAAGCTGCGG-3′ and 5′-CCGCAAGCTTTCCATTTATGCGG-TAG-3′. The PCR product was digested with *EcoR*I and *Hind*III, and then cloned into the *EcoRI*/*Hind*III site of the expression vector pET32a (Novagen). The mixture of $3CL^{pro}$ and vacuolar-H^+ ATPase thioredoxin fusion protein was first incubated with anti-thioredoxin mAb (Invitrogen) for 4 h at 4 °C, and then reacted with the protein A-Sepharose beads for the addition of 2-h incubation. After centrifugation, the pellet was washed four times with NET buffer (150 mM NaCl, 0.1 mM EDTA, 30 mM Tris–HCl, and pH 7.4). The immunoprecipitate was dissolved in a 2× SDS–PAGE sample buffer without 2-mercaptoethanol and boiled for 10 min. Proteins were resolved on 12% SDS–PAGE gels and electrophoretically transferred to nitrocellulose papers. The resultant blots were blocked with 5% skim milk, and then reacted with the anti-His tag mAb for 1-h incubation. The blots were then washed with TBS three times and overlaid with a 1/1000 dilution of rabbit anti-mouse IgG antibodies conjugated with alkaline phosphatase (KPL). Following another1-h incubation at room temperature, the blots were developed with NBT/BCIP (Invitrogen).

2.3. ELISA affinity assay

The wells of a 96-well microtiter plate were coated with 100 μl of 5 μg/ml $3CL^{pro}$ and were incubated at 4 °C overnight. Following each incubation and subsequent layer of the enzyme-linked immunosorbent assay (ELISA), the wells were washed three times with TBS containing 0.05% Tween 20 (TBST). After blocking with 5% skim milk in TBST, serial dilution of V-ATPase G1 TRX fusion protein or thioredoxin (TRX) was incubated in $3CL^{pro}$-coated wells for 2 h. The bound V-ATPase G1 TRX fusion protein or TRX protein was detected with the anti-TRX monoclonal antibody, and then the ELISA product was developed with goat anti-mouse IgG-HRP conjugate and ABTS/H_2O_2 substrates. The relative affinity, K_d, was estimated from the concentration necessary for 50% maximal binding based on a computer program employing Fisher's statistical model.

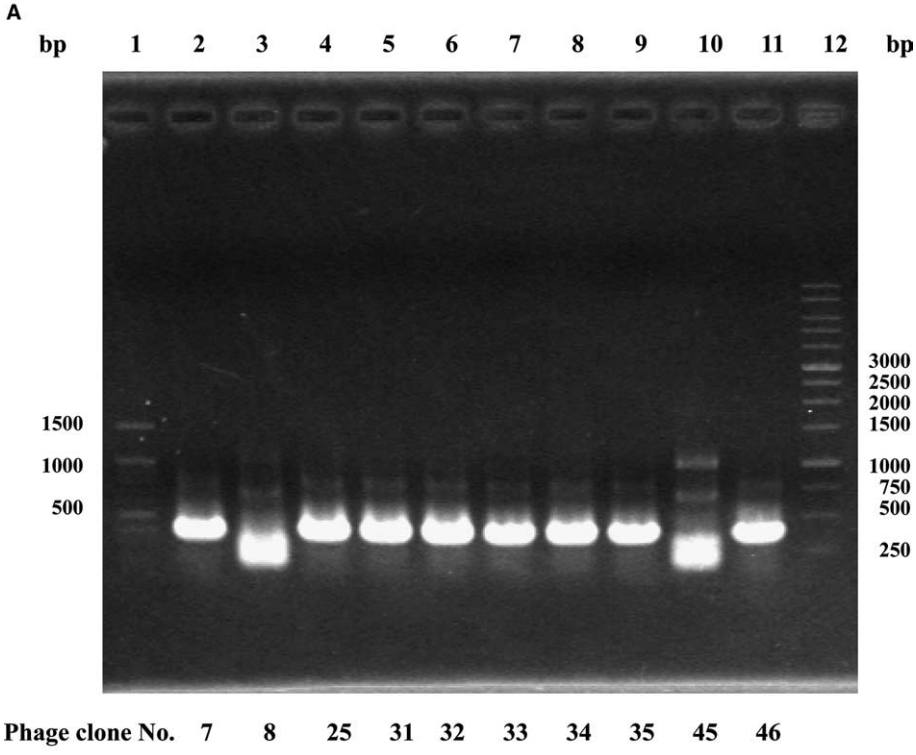

Fig. 1. Gel electrophoresis of PCR products (A) and deduced amino acid sequence (B) from SARS-CoV $3CL^{pro}$-interacting human lung proteins displayed on the identified phage clones. (A) After five rounds of biopanning with SARS-CoV $3CL^{pro}$, the human lung cDNA clones displayed on individual eluted phage plaques were amplified using PCR. (B) The amino acid sequence of $3CL^{pro}$-interacting human lung protein that was identified from phage Nos. 7, 25, 31, 32, 33, 34, 35, and 46 was deduced from the human lung cDNA nucleotide sequence from $3CL^{pro}$-interacting phage No. 7. A dashed-line box was marked for the possible $3CL^{pro}$ cleavage site.

2.4. Trans-cleavage of V-ATPase G1 by SARS-CoV 3CL^{pro} protease

The SARS-CoV 3CL^{pro} protease was incubated with the V-ATPase G1 TRX fusion protein or TRX protein in 100 mM Tri–HCl (pH 9.0) at 37 °C. The proteolytic processing was analyzed using Western blotting with anti-His tag antibody. Band intensities of the V-ATPase G1 TRX fusion protein or TRX protein on the nitrocellulose were quantified by densitometric analysis.

2.5. Immunoprecipitates of cell extract by 3CL^{pro}

The 3CL^{pro} gene was cloned into the pcDNA3.1 vector and generated as a His-tag fusion protein [17]. The resulting plasmid pcDNA3.1-SARS CoV 3CL^{pro} (pSARS-CoV 3CL^{pro}) (4.5 μg) plus indicator vector pEGFP-N1 (0.5 μg) was transfected into HL-CZ cells, a human promonocyte cell line [19], using the GenePorter reagent. The cell extract of the 3CL^{pro}-expressing cells and mock cells was incubated with anti-His tag antibody to 3CL^{pro} for 4 h at 4 °C, and then reacted with the protein A-Sepharose beads for the addition of 2-h incubation. The immunoprecipitate was analyzed using Coomassie blue staining, and Western blotting with anti-His tag antibody to 3CL^{pro} and chicken anti-V-ATPase G1 polyclonal antibody (Chemicon).

2.6. Measurement of intracellular pH in transfected cells with SNARF-1

Transfected cells were washed three times with PBS and incubated with 20 μM carboxy SNARF-1 (Molecular Probe) for 30 min at room temperature. Subsequently, the cells were washed with PBS again and then placed into the microplates. A dual-emission ration at 580 and 640 nm of intracellular dye was detected using a fixed excitation at 514 nm, and then converted to intracellular pH (pH_i) according to previous reports [20].

3. Results

3.1. Identification of SARS-CoV 3CL^{pro}-interacting lung protein(s)

For identifying potential 3CL^{pro}-interacting human lung proteins, affinity selection of a phage-displayed human lung cDNA library with recombinant 3CL^{pro} protein was carried out. After five rounds of biopanning, fifty eluted phage plaques were selected for determining relative affinities to SARS-CoV 3CL^{pro} using direct binding ELISA assay. Ten of the fifty phage clones, phage-7, 8, 25, 31, 32, 33, 34, 35, 45, and 46 had higher absorbance values of the ELISA product compared to other phage clones (data not shown here). In addition, these ten selected phage clones showed approximately 3–5-fold increases in direct ELISA binding compared to the wild type phage T7. Therefore, these ten identified phage clones were suggested to display the high affinity of lung cDNA clones to SARS-CoV 3CL^{pro}.

Lung cDNA clones displayed on these ten 3CL^{pro}-interacting phages were subsequently amplified using PCR. Gel electrophoresis of the PCR products revealed that about 400 base pair products were amplified from eight phage clones, phage-7, 25, 31, 32, 33, 34, 35, and 46 (Fig. 1A, lanes 2, 4, 5, 6, 7, 8, 9, and 11), and about 300 pair products were found in two phage clones, phage-8 and 45 (Fig. 1A, lanes 3 and 10). Direct sequencing of the PCR products showed the same nucleotide sequences of lung cDNA clones displayed on phage-7, 25, 31, 32, 33, 34, 35, and 46 (Fig. 1B). The BLAST alignment search indicated that the deduced amino acid sequence of the 3CL^{pro}-interacting lung cDNA clone was identical to the C-terminus of vacuolar ATP synthase subunit G 1 (V-ATPase G1 subunit) (GenBank Accession No. O75348 and NP_004879). Interestingly, V-ATPase G1 contains a motif Thr-Ile-Leu-Gln-Thr, being similar to the conserved 3CL^{pro} cleavage sites (Val/Thr)-X-Leu-Gln-(Ser/Ala).

3.2. Binding interaction of 3CL^{pro} with V-ATPase G1

To test the specific interaction of 3CL^{pro} with V-ATPase G1, the identified lung cDNA clone encoding for the C-terminus of V-ATPase G1 subunit was cloned into the bacterial expression vector pET32a, being generated as a thioredoxin (TRX) and His-tag fusion protein in *E. coli*. Co-immunoprecipitation of

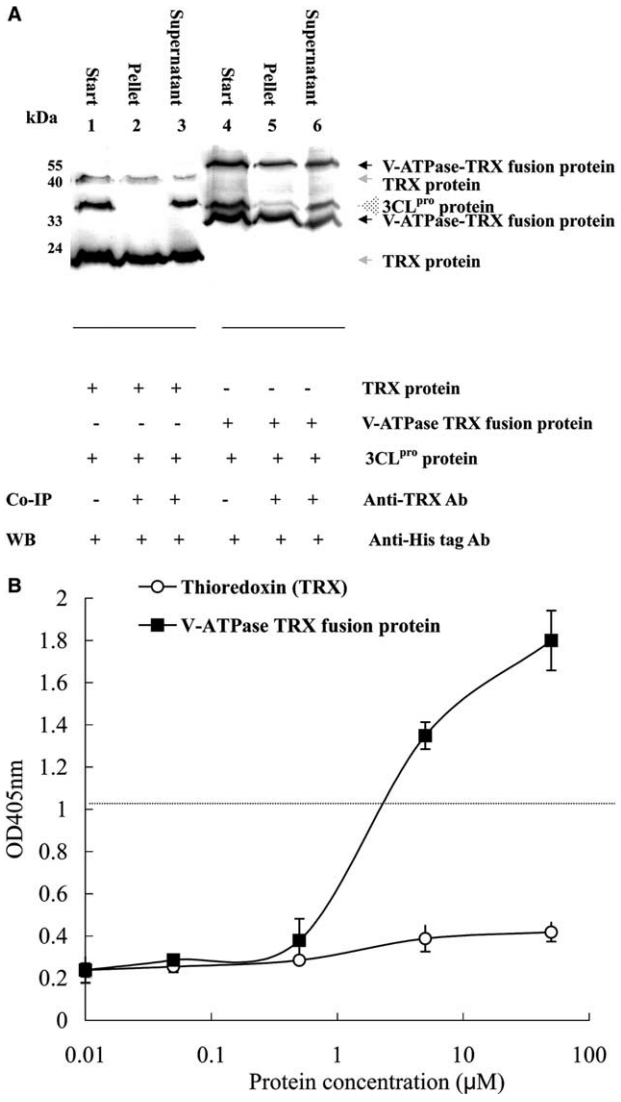

Fig. 2. The specific interaction of SARS-CoV 3CL^{pro} with V-ATPase G1 TRX fusion protein using co-immunoprecipitation assay (A) and the binding affinity assay (B). (A) An equal amount of V-ATPase G1 TRX fusion protein and the SARS-CoV 3CL^{pro} was first incubated with anti-TRX mAb at 4 °C overnight, followed by incubation with the protein A-Sepharose beads for the addition of 2-h incubation. After centrifugation, the pellet was washed with NET buffer, and then dissolved in 2× SDS–PAGE sample buffer without 2-mercaptoethanol and boiled for 10 min. Following the western blot procedure, the blot was probed with mouse anti-His tag antibodies, and developed with an alkaline phosphatase-conjugated secondary antibody and NBT/BCIP substrates. (B) 100 μl of 5 μg/ml 3CL^{pro} was coated onto 96-well plates; followed by incubation with the indicated concentration of V-ATPase G1 TRX fusion protein or thioredoxin (TRX). Bound V-ATPase G1 TRX fusion protein or thioredoxin was detected using anti-TRX monoclonal antibody. The ELISA product was developed with goat anti-mouse IgG-HRP conjugate and ABTS/H_2O_2 substrates.

the 3CL^{pro} protein with the V-ATPase G1 TRX fusion protein was performed. After centrifugation, the protein complex was precipitated by the anti-thioredoxin antibody and the protein A-Sepharose beads. Western blot analysis of the immunoprecipitate demonstrated that 3CL^{pro} was precipitated by the V-ATPase G1 TRX fusion protein (Fig. 2A, lane 5) but not the TRX protein (Fig. 2A, lane 2). Furthermore, direct binding of V-ATPase G1 TRX fusion protein to SARS-CoV 3CL^{pro} showed a dose-dependent manner in the ELISA assay (Fig. 2B). The relative binding affinity (K_d) of the V-ATPase G1 TRX fusion protein to recombinant 3CL^{pro} protease was approximately 1.9 μM, indicating that the V-ATPase G1 subunit was sufficient for binding to SARS-CoV 3CL^{pro}.

3.3. Cleavage of V-ATPase G1 by SARS-CoV 3CL^{pro}

Because the V-ATPase G1 contains a possible cleavage site for 3CL^{pro}, the *trans*-cleavage reaction of 3CL^{pro} with the V-ATPase G1 TRX fusion protein was carried out in the alkaline buffer at 37 °C. In Western blot analysis with anti-His tag antibody, the V-ATPase G1 TRX fusion protein but not the TRX protein was cleaved by the 3CL^{pro} protease (Fig. 3). Based on the remaining amount of the V-ATPase G1 TRX fusion protein, densitometric analysis demonstrated that the percentage of the cleaved V-ATPase G1 TRX fusion protein reached up to approximately 70% (Fig. 3, lanes 7–9); however, no significant change was found in the amount of the TRX protein (Fig. 3, lanes 3–5).

3.4. Interaction of SARS-CoV 3CL^{pro} with cellular V-ATPase G1

To examine the cell-based interaction of SARS-CoV 3CL^{pro} with V-ATPase G1, the SARS-CoV 3CL^{pro} gene was cloned into the mammalian expression vector pcDNA3.1, and then transfected into human promonocyte HL-CZ cells. Western blotting analysis of cell lysates with anti-His-tag antibody demonstrated a major 68-kDa band for the dimer and a minor 34-kDa band in the 3CL^{pro}-expressing cells (not shown here). For further analyzing the binding of cellular V-ATPase G1 to 3CL^{pro}, the cell lysate of the 3CL^{pro}-expressing cells and mock cells was precipitated by anti-His tag antibody to 3CL^{pro} (Fig. 4A–C). In the Coomassie-stained gel, the immunoprecipitate by anti-His tag antibody contained many cellular proteins from the 3CL^{pro}-expressing cells (Fig. 4A, lane 6), while only a few proteins from mock cells (Fig. 4A, lane 3). Of the cellular proteins in the immunoprecipitate, a 68-kDa – immunoreactive band for the dimer 3CL^{pro} was found using Western blotting with anti-His tag antibody (Fig. 4B, lane 6). In addition, Western blot analysis with anti-V-ATPase G1 polyclonal antibodies demonstrated a major 13-kDa band for cellular V-ATPase G1 protein in the 3CL^{pro}-precipitated pellet (Fig. 4C, lane 6). The result confirmed the interaction between 3CL^{pro} and V-ATPase G1 in the HL-CZ cells. Since V-ATPase in the plasma and lysosomal membranes is the major proton-extruding molecule for controlling cytosolic pH_i [21,22], the cytosolic pH_i in SARS-CoV 3CL^{pro} – expressing cells and pcDNA3.1-expressing cells was determined by the fluorescence of SNARF-1 (Fig. 4D). Cytosolic pH_i of SARS-CoV 3CL^{pro} – expressing cells ($pH_i = 7.70 \pm 0.002$) was significantly lower (*t* test, $P < 0.05$) than that of pcDNA3.1-expressing cells ($pH_i = 7.79 \pm 0.009$).

4. Discussion

V-ATPase G subunit 1 was identified as a SARS-CoV 3CL^{pro}-interacting protein by the affinity selection of a phage-displayed human lung cDNA library (Fig. 1). Co-immunoprecipitation analysis and direct binding affinity demonstrated the specific interaction of 3CL^{pro} with V-ATPase G subunit 1 (Figs. 2 and 4). V-ATPase resides on the membranes of acidic organelles such as secretary granules, lysosomes, and the *trans*-Golgi network, being the major proton-extruding molecule for maintaining acidic environment [21–25]. V-ATPase is a multisubunit complex with two functional domains, namely, the peripheral V_1 domain and the integral V_0 domain. V-ATPase G subunit 1 belongs to the accessory V1 subunits, being responsible for ATP hydrolysis. Interestingly, human papillomavirus 16 (HPV16) E5 protein has been demonstrated to bind to the 16-kDa subunit of the vacuolar H(+)-ATPase (16 K) [26], and to inhibit the assembly, stability and complex formation of the V-ATPase [27]. Our findings are in agreement with the previous reports [26,27] showing that

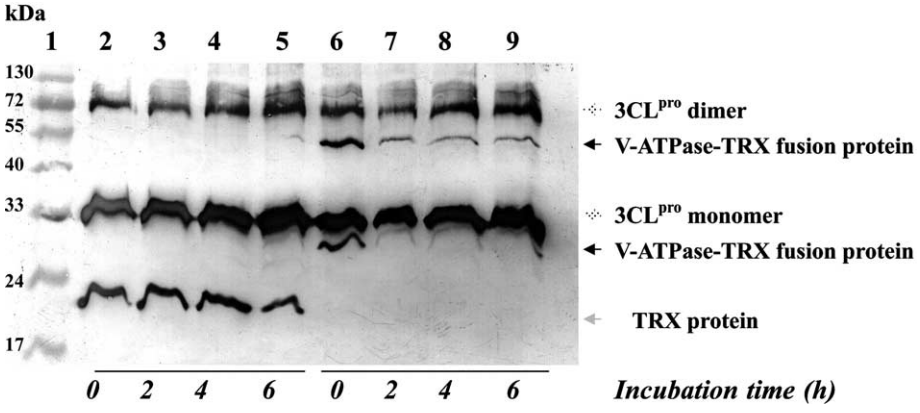

Fig. 3. *Trans*-cleavage of V-ATPase G1 TRX fusion protein by SARS-CoV 3CL^{pro} protease. The SARS-CoV 3CL^{pro} protease was incubated with the V-ATPase G1 TRX fusion protein (lanes 6–9) or TRX protein (lanes 2–5) in 100 mM Tris–HCl, (pH 9.0) at 37 °C, and the proteolytic processing was analyzed using Western blotting with anti-His tag antibody. Lane 1, protein markers.

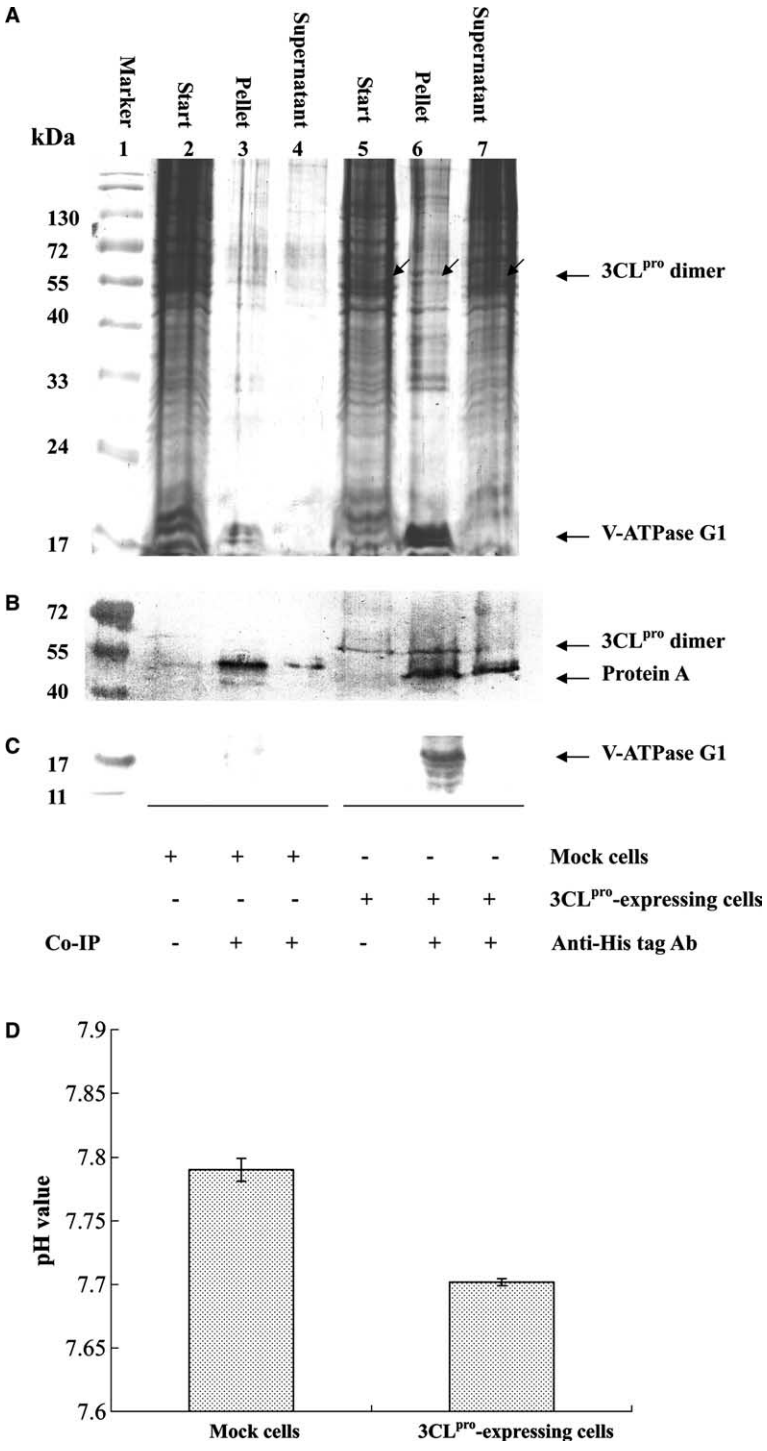

Fig. 4. Cell-based co-immunoprecipitation (A–C) and decrease intracellular pH (D) by SARS-CoV 3CL^{pro} protease. The cell lysates of 3CL^{pro}-expressing cells and mock cells were immunoprecipitated by anti-His tag to 3CL^{pro}. The immunoprecipitate was analyzed using Coomassie blue staining (A), and Western blotting with anti-His tag antibody to 3CL^{pro} (B) and chicken anti-V-ATPase G1 polyclonal antibody (C). In addition, the 3CL^{pro}-expressing cells and mock cells were incubated with 20 μM carboxy SNARF-1 for 30 min at room temperature. A dual-emission ration at 580 and 640 nm of intracellular dye was detected using a fixed excitation at 514 nm, and then converted to intracellular pH (D).

vacuolar H(+)-ATPase can be involved in the virus-induced pathogenesis.

Cleavage of the V-ATPase G1 fusion protein by SARS-CoV 3CL^{pro} was found in this study (Fig. 3), implying that 3CL^{pro} potentially cleaves the cellular V-ATPase G1, and affects the function of vacuolar H(+)-ATPase. Meanwhile, a significant intracellular acidification has been demonstrated in the 3CL^{pro}-expressing cells (Fig. 4D). The result correlated well with previous reports in that V-ATPase-specific inhibitors cause acidic pH_i [28,29], and influences cell apoptosis [30,31]. Recent studies demonstrate the binding interaction of V-ATPase with F-actin, being important for regulating in response to

phosphatidylinositol 3-kinase activity [32]. Comparing to the immunoprecipitate of mock cell extract by anti-His tag antibody (Fig. 4A, lane 3), significantly more proteins were precipitated in the $3CL^{pro}$-expressing cells (Fig. 4A, lane 6), in which some proteins such as F-actin could be brought down by V- ATPase G1.

In conclusion, a phage displayed library encoding sequences from human lung cDNA was used to identify potential $3CL^{pro}$-interacting lung proteins. V-ATPase G1 was identified as a $3CL^{pro}$-interacting protein in this study. The interaction of $3CL^{pro}$ with V-ATPase G1 resulted in the cleavage of V-ATPase G1. This interaction is likely to be involved in the virus-induced pathogenesis.

Acknowledgments: We thank the National Science Council (Taiwan) and China Medical University for financial supports (NSC93-2320-B-039-051, 93-2745-B-039-004-URD, and CMU-93-MT-04).

References

[1] Nicholls, J.M., Poon, L.L., Lee, K.C., Ng, W.F., Lai, S.T., Leung, C.Y., Chu, C.M., Hui, P.K., Mak, K.L., Lim, W., Yan, K.W., Chan, K.H., Tsang, N.C., Guan, Y., Yuen, K.Y. and Peiris, J.S. (2003) Lung pathology of fatal severe acute respiratory syndrome. Lancet 361, 1773–1778.

[2] Lang, Z., Zhang, L., Zhang, S., Meng, X., Li, J., Song, C., Sun, L. and Zhou, Y. (2003) Pathological study on severe acute respiratory syndrome. Chin. Med. J. (Engl). 116, 976–980.

[3] Wang, W.K., Chen, S.Y., Liu, I.J., Kao, C.L., Chen, H.L., Chiang, B.L., Wang, J.T., Sheng, W.H., Hsueh, P.R., Yang, C.F., Yang, P.C. and Chang, S.C. (2004) Temporal relationship of viral load, ribavirin, interleukin (IL)-6, IL-8, and clinical progression in patients with severe acute respiratory syndrome. Clin. Infect Dis. 39, 1071–1075.

[4] Huang, K.J., Su, I.J., Theron, M., Wu, Y.C., Lai, S.K., Liu, C.C. and Lei, H.Y. (2005) An interferon-gamma-related cytokine storm in SARS patients. J. Med. Virol. 75, 185–194.

[5] Lai, M.M.C. and Holmes, K.V. (2001) Coronaviridae: the viruses and their replication in: Fields Virology (Knipe, D.M. and Howley, P.M., Eds.), Lippincott Williams and Wilkins, New York.

[6] Enjuanes, L., Brian, D., Cavanagh, D., Holmes, K., Lai, M.M.C., Laude, H., Masters, P., Rottier, P., Siddell, S.G., Spaan, W.G.M., Taguchi, F. and Talbot, P. (2000) Coronaviridae in: Virus Taxonomy (van Regenmortal, M.H.V., Fauqet, C.M., Bishop, E.B., Carstens, E.B., Estes, M.K., Lemon, S.M., Mayo, M.A., McGeoch, D.J., Pringle, C.R. and Wickner, R.B., Eds.), Academic Press, New York.

[7] Holmes, K.V. (2001) Coronaviruses in: Fields Virology (Knipe, D.M. and Howley, P.M., Eds.), Lippincott Williams and Wilkins, New York.

[8] Ziebuhr, J., Snijder, E.J. and Gorbalenya, A.E. (2000) Virus-encoded proteinases and proteolytic processing in the Nidovirales. J. Gen. Virol. 81, 853–879.

[9] Yalamanchili, P., Weidman, K. and Dasgupta, A. (1997) Cleavage of transcriptional activator Oct-1 by poliovirus encoded protease 3Cpro. Virology 239, 176–185.

[10] Yalamanchili, P., Datta, U. and Dasgupta, A. (1997) Inhibition of host cell transcription by poliovirus: cleavage of transcription factor CREB by poliovirus-encoded protease 3Cpro. J. Virol. 71, 1220–1226.

[11] Urzainqui, A. and Carrasco, L. (1989) Degradation of cellular proteins during poliovirus infection: studies by two-dimensional gel electrophoresis. J. Virol. 63, 4729–4735.

[12] Blom, N., Hansen, J., Blaas, D. and Brunak, S. (1996) Cleavage site analysis in picornaviral polyproteins: discovering cellular targets by neural networks. Protein Sci. 5, 2203–2216.

[13] Calandria, C., Irurzun, A., Barco, A. and Carrasco, L. (2004) Individual expression of poliovirus 2Apro and 3Cpro induces activation of caspase-3 and PARP cleavage in HeLa cells. Virus Res. 104, 39–49.

[14] Li, M.L., Hsu, T.A., Chen, T.C., Chang, S.C., Lee, J.C., Chen, C.C., Stollar, V. and Shih, S.R. (2002) The 3C protease activity of enterovirus 71 induces human neural cell apoptosis. Virology 293, 386–395.

[15] Funkhouser, A.W., Kang, J.A., Tan, A., Li, J., Zhou, L., Abe, M.K., Solway, J. and Hershenson, M.B. (2004) Rhinovirus 16 3C protease induces interleukin-8 and granulocyte-macrophage colony-stimulating factor expression in human bronchial epithelial cells. Pediatr Res. 55, 13–18.

[16] Kiemer, L., Lund, O., Brunak, S. and Blom, N. (2004) Coronavirus 3CLpro proteinase cleavage sites: possible relevance to SARS virus pathology. BMC Bioinformatics 5, 72.

[17] Lin, C.W., Tsai, C.H., Tsai, F.J., Chen, P.J., Lai, C.C., Wan, L., Chiu, H.H. and Lin, K.H. (2004) Characterization of *trans*- and *cis*-cleavage activity of the SARS coronavirus 3CLpro protease: basis for the in vitro screening of anti-SARS drugs. FEBS Lett. 574, 131–137.

[18] Liu, W.T., Chen, C.L., Lee, S.S., Chan, C.C., Lo, F.L. and Ko, Y.C. (1991) Isolation of dengue virus with a human promonocyte cell line. Am. J. Trop. Med. Hyg. 44, 494–499.

[19] Lin, C.W. and Wu, S.C. (2004) Identification of mimotopes of the Japanese encephalitis virus envelope protein using phage-displayed combinatorial peptide library. J. Mol. Microbiol. Biotechnol. 8, 34–42.

[20] Martinez-Zaguilan, R., Raghunand, N., Lynch, R.M., Bellamy, W., Martinez, G.M., Rojas, B., Smith, D., Dalton, W.S. and Gillies, R.J. (1999) pH and drug resistance. II. Turnover of acidic vesicles and resistance to weakly basic chemotherapeutic drugs. Biochem. Pharmacol. 57, 1037–1046.

[21] Swallow, C.J., Grinstein, S. and Rotstein, O.D. (1990) A vacuolar type H(+)-ATPase regulates cytoplasmic pH in murine macrophages. J. Biol. Chem. 265, 7645–7654.

[22] Conboy, I.M., Manoli, D., Mhaiskar, V. and Jones, P.P. (1999) Calcineurin and vacuolar-type H+-ATPase modulate macrophage effector functions. Proc. Natl. Acad. Sci. USA 96, 6324–6329.

[23] Bidani, A., Reisner, B.S., Haque, A.K., Wen, J., Helmer, R.E., Tuazon, D.M. and Heming, T.A. (2000) Bactericidal activity of alveolar macrophages is suppressed by V-ATPase inhibition. Lung 178, 91–104.

[24] Fan, K., Wei, P., Feng, Q., Chen, S., Huang, C., Ma, L., Lai, B., Pei, J., Liu, Y., Chen, J. and Lai, L. (2004) Biosynthesis, purification, and substrate specificity of severe acute respiratory syndrome coronavirus 3C-like proteinase. J. Biol. Chem. 279, 1637–1642.

[25] Nelson, N. (1991) Structure and pharmacology of the proton-ATPases. Trends Pharmacol. Sci. 12, 71–75.

[26] Gieswein, C.E., Sharom, F.J. and Wildeman, A.G. (2003) Oligomerization of the E5 protein of human papillomavirus type 16 occurs through multiple hydrophobic regions. Virology 313, 415–426.

[27] Briggs, M.W., Adam, J.L. and McCance, D.J. (2001) The human papillomavirus type 16 E5 protein alters vacuolar H(+)-ATPase function and stability in *Saccharomyces cerevisiae*. Virology 280, 169–175.

[28] Conboy, I.M., Manoli, D., Mhaiskar, V. and Jones, P.P. (1999) Calcineurin and vacuolar-type H^+-ATPase modulate macrophage effector functions. Proc. Natl. Acad. Sci. USA 96, 6324–6329.

[29] Heming, T.A. and Bidani, A. (2003) Intracellular pH regulation in U937 human monocytes: roles of V-ATPase and Na^+/H^+ exchange. Immunobiology 207, 141–148.

[30] Yoshimoto, Y. and Imoto, M. (2002) Induction of EGF-dependent apoptosis by vacuolar-type H(+)-ATPase inhibitors in A431 cells overexpressing the EGF receptor. Exp. Cell Res. 279, 118–127.

[31] Xu, J., Feng, H.T., Wang, C., Yip, K.H., Pavlos, N., Papadimitriou, J.M., Wood, D. and Zheng, M.H. (2003) Effects of Bafilomycin A1: an inhibitor of vacuolar H (+)-ATPases on endocytosis and apoptosis in RAW cells and RAW cell-derived osteoclasts. J. Cell Biochem. 88, 1256–1264.

[32] Chen, S.H., Bubb, M.R., Yarmola, E.G., Zuo, J., Jiang, J., Lee, B.S., Lu, M., Gluck, S.L., Hurst, I.R. and Holliday, L.S. (2004) Vacuolar H^+-ATPase binding to microfilaments: regulation in response to phosphatidylinositol 3-kinase activity and detailed characterization of the actin-binding site in subunit B. J. Biol. Chem. 279, 7988–7998.